Spatial and Temporal Variability of Canadian Seasonal Streamflows

PAULIN COULIBALY

Department of Civil Engineering and School of Geography and Geology, McMaster University, Hamilton, Ontario, Canada

DONALD H. BURN

Department of Civil Engineering, University of Waterloo, Waterloo, Ontario, Canada

(Manuscript received 9 December 2003, in final form 7 June 2004)

ABSTRACT

Wavelet and cross-wavelet analysis are used to identify and describe spatial and temporal variability in Canadian seasonal streamflows, and to gain insights into the dynamical relationship between the seasonal streamflows and the dominant modes of climate variability in the Northern Hemisphere. Results from applying continuous wavelet transform to mean seasonal streamflows from 79 rivers selected from the Canadian Reference Hydrometric Basin Network (RHBN) reveal striking climate-related features before and after the 1950s. The span of available observations, 1911–99, allows for depicting variance and covariance for periods up to 12 yr. Scale-averaged wavelet power spectra are used to simultaneously assess the temporal and spatial variability in each set of 79 seasonal streamflow time series. The most striking feature, in the 2–3-yr period and in the 3–6-yr period—the 6–12-yr period is dominated by white noise and is not considered further—is a net distinction between the timing and intensity of the temporal variability in autumn, winter, and spring–summer streamflows. It is found that the autumn season exhibits the most intense activity (or variance) in both the 2–3- and the 3–6-yr periods. The spring–summer season corresponds to the least intense activity for the 2–3-yr period, but it exhibits more activity than winter for the 3–6-yr period.

Cross-wavelet analysis is provided between the seasonal streamflows and three selected climatic indices: the Pacific–North America (PNA), the North Atlantic Oscillation (NAO), and the sea surface temperature series over the Niño-3 region (ENSO3). The wavelet cross-spectra reveal strong climate–streamflow activity (or covariance) in the 2–6-yr period starting after 1950 whatever the climatic index and the season. Prior to 1950, local and weaker 2–6-yr activity is revealed in central and western Canada essentially in winter and autumn, but overall a non-significant streamflow–climate relationship is observed prior to 1950. Correlation analysis in the 2–6-yr band between the seasonal streamflow and the selected climatic indices revealed strong positive correlations with the ENSO in the spring–summer and winter seasons for the post-1950 period for both eastern and western Canada. A similar correlation pattern is revealed in the west with the NAO, while in the east moderate negative NAO correlations are observed only in the autumn season prior to 1950. After 1950 strong NAO correlations emerge for all the seasons. The cross-wavelet spectra and the correlation analysis in the 2–6-yr band suggest the presence of a change point around 1950 in the east and west seasonal streamflows.

1. Introduction

Hydrological systems act as sensible spatial and temporal integrators of precipitation (rain and snow), temperature, and related evaporation over a specific area or region. Seasonal variations of streamflows arise from variations in precipitation and temperature, which are controlled by large-scale fluctuations in atmospheric circulation patterns. Hence, streamflow records can serve as a pertinent index of hydroclimatic variability at a local or regional scale. Gaining insight into the finer temporal structures of streamflow variability is essential to the understanding of the complex hydrology–climate relationship and the dynamics of the hydrologic cycle, which in turn will improve our ability in modeling hydrological systems. This typically requires a decomposition of streamflow time series into time–frequency space to identify the dominant modes of variability and to determine how these modes vary in time. This has been done by resorting mostly to Fourier transforms (Hameed 1984; Kunhel et al. 1990; Larocque et al. 1998). A major limitation of the Fourier analysis is that it does not retain the location of a particular event in time and space, nor does it perform well on irregularly spaced events or nonstationary signals (Smith et al.

Corresponding author address: P. Coulibaly, Dept. of Civil Engineering and School of Geography and Geology, McMaster University, Hamilton, ON L8S 4L7, Canada.
E-mail: couliba@mcmaster.ca

1998). Standard short-term Fourier transform is particularly limited by its window of fixed arbitrary length. It has been recently shown that temporal structures of rainfall–runoff records cannot be taken into account adequately using classical spectral or correlation analyses (Labat et al. 2000a). As an alternative, wavelet transforms have been proposed. A major property of the wavelet transform is its ability to provide a robust approach to decompose and represent time series into a finer scale–time domain without a window with arbitrary limited length. Furthermore, it can permit distinguishing between two signals that have very similar Fourier spectra.

Wavelet analysis has been used in geophysics and meteorology to identify coherent convective storm structures and characterize their temporal variability (Kumar and Foufoula-Georgiou 1993; Takeuchi et al. 1994; Kumar 1996; Szilagyi et al. 1999) or to analyze localized variations within geophysical time series including climatic indices (Shabbar et al. 1997b; Hu et al. 1998; Lucero and Rodriguez 1999). In hydrology, wavelet analysis has been recently applied to examine daily rainfall–runoff relationships in a karstic watershed (Labat et al. 2000b), and also to characterize daily streamflow in the United States (Smith et al. 1998) and to describe reservoir inflow variability in northern Quebec (Coulibaly et al. 2000). More recently, wavelet analysis has been used to describe interannual variability in southern Quebec streamflows (Anctil and Coulibaly 2004). The last two studies were not only confined to a specific region but also limited to about 50 years of mean annual flows.

In this analysis, continuous wavelet transforms are used to allow a finer analysis of the time-varying structures of the seasonal streamflow records and the streamflow–climate relationship throughout Canada. The main objectives of this analysis are to describe and document the seasonal variability in Canadian streamflows using wavelet and cross-wavelet analysis. This study also aims to examine the role of the dominant climatic patterns in the Northern Hemisphere on the seasonal variability of Canadian streamflows. The remainder of the paper is organized as follows. A description of the study area and the datasets are first provided. The continuous wavelet and cross-wavelet analysis method is presented next. Results from the wavelet analysis are then reported, and finally some conclusions are drawn.

2. Study area and datasets

a. Reference Hydrometric Basin Network (RHBN)—Seasonal streamflows

The analysis described herein was performed on stations from the Reference Hydrometric Basin Network (RHBN), a data collection network of natural rivers in Canada identified by Environment Canada for climatic change research. The criteria according to which stations were selected for the RHBN are as follows (Harvey et al. 1999):

1) degree of basin development: Stations that were included in the network were those that reflect catchments that are pristine or have stable land-use conditions.
2) absence of significant regulations or diversions: A catchment was considered natural if there was no control structure upstream of the gauging station, while it was considered regulated if there was an upstream control structure.
3) record length: A station must have a minimum record length of 20 years to be included in the RHBN. The present work selected from the RHBN only those stations with a record length of at least 35 years to ensure an adequate record length for the wavelet analysis.
4) longevity: This criterion was based on the judgment of the regional staff. A station was excluded from the network if it is currently active but was expected not to have future data collection activities.
5) data accuracy: Data accuracy was assessed qualitatively by local experts based on knowledge of the hydraulic condition of the stations to ensure that only stations with good quality data were included in the network.

Basin sizes in the RHBN range from 3.63 to 145 000 km^2 with a median size of 1170 km^2; 10% of the basins have a drainage area greater than 20 000 km^2, and 10% have a drainage area less than 100 km^2. An analysis of the characteristics of stations within the RHBN indicates certain limitations of the existing network. The network tends to comprise large basins in the north and smaller basins in the south, and certain provinces have large gaps in spatial coverage.

The current research employs a subset of the RHBN consisting of 79 longer-term gauging stations (see Fig. 1) to minimize the limited data record problem and allow longer period (up to decadal time scale) analysis. The subset of the RHBN that has been selected for this work suffers from the same limitations outlined above for the RHBN as a whole. In particular, there are a limited number of stations representing the Canadian north and there are few stations from the Prairie Provinces (or central Canada). The median record length for the stations analyzed in this work is 49 years, with a range of record lengths from 35 to 85 years. The catchment drainage areas range from 3.63 to 29 900 km^2 with a median value of 1350 km^2. As such, the subset of the RHBN is fairly typical of the stations in the RHBN in terms of drainage areas, but consists only of the best available streamflow time series with longer record lengths. The selected sites along with the station numbers, drainage basin areas, and locations are listed in Table 1. The regional grouping of sites (Table 1) is

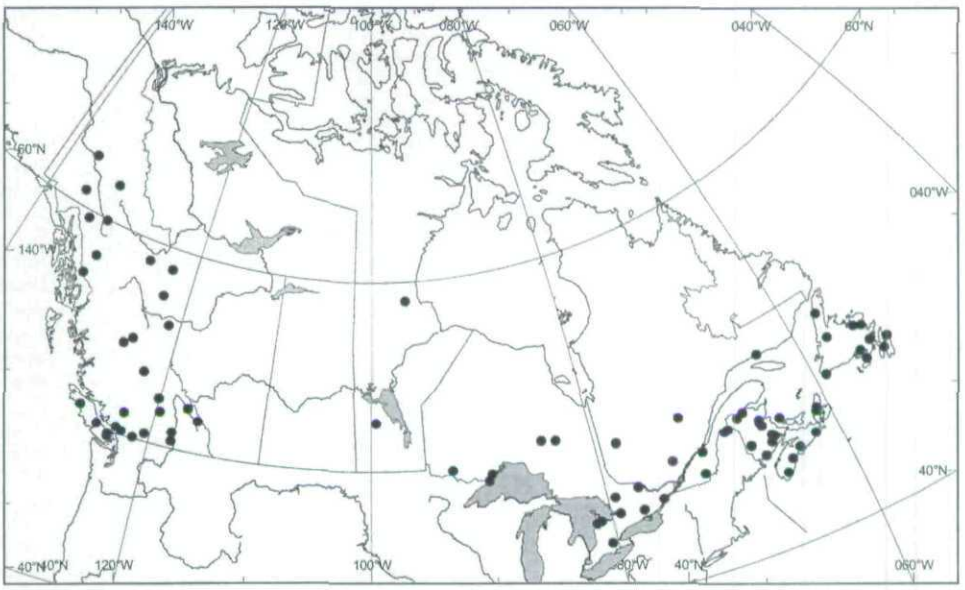

FIG. 1. Location map: Canada RHBN of the 79 flow stations selected.

based on statistical analysis and climatic factors (Harvey et al. 1999; Adamowski and Bocci 2001). The hydrologic variable selected for this research is the seasonal mean flow, given that the study is mainly concerned with the strong seasonal variability inherent to Nordic river flows. Owing to the large size of the study area, the length of season is region dependent. Hence seasonal division of streamflow is based on the analysis of all the monthly streamflow available in each region. To illustrate the streamflow division, Fig. 2 shows the distribution of monthly flow for two stations (02YL001 and 02KB001—located in Upper Humber River, Newfoundland, and in Petawawa River, Ontario, respectively) and the seasonal division of streamflow adopted. Similar analysis was conducted for each of the nine climatic regions. Table 2 presents the seasonal division of streamflow for each region and the seasonal climatic indices used in this study and described hereafter.

b. *Climatic indices*

The analysis also includes several climatic patterns that appear and persist in the Northern Hemisphere. Two of these are the North Atlantic Oscillation (NAO) and the Pacific–North American (PNA), which are found to be the most prominent and recurrent patterns of atmospheric circulation variability in the Northern Hemisphere (e.g., storm-track and temperature changes; Barnston and Livezey 1987; National Research Council 1998; Hurrell et al. 2003). The NAO is a large-scale alternation of atmospheric mass with centers of action near the Icelandic low and the Azores high. It is the dominant and persistent mode of atmospheric behavior in the North Atlantic throughout the year explaining on average 32% of the variance in monthly sea level pressures (SLP) (Cayan 1992) but with even greater dominance during the winter. The NAO index used in this study is from Hurrell (1995) who exploited SLP anomalies from Lisbon, Portugal, and Stykkisholmur, Iceland. While exhibiting considerable interannual variability with concentrations of spectral power around periods of 2.1, 8, and 24 yr (Cook et al. 1998), the NAO has been in a generally positive phase since about 1970. A significant coherent relationship between the NAO and the North Atlantic sea surface temperature has recently been found at interannual and interdecadal time scales (Higuchi et al. 1999). The signature of the NAO is strongly regional and can be directly tied to variations in regional precipitation. Therefore the NAO index may be a relevant variable to the regional hydrology. For example, in a study on interannual variability of Canadian snow cover from 1915 to 1992 (Brown and Goodison 1996), significant winter NAO–snow cover correlations were observed in Ontario and southern Quebec, specifically in December. Other studies (Coulibaly et al. 2000; Anctil and Coulibaly 2004) have shown the influence of the NAO circulation pattern on annual flow in northern and southern Quebec.

Another persistent climatic pattern that has to be considered in the Northern Hemisphere is the Pacific–North American atmospheric teleconnection, which is defined as a measure of atmospheric response to a warm sea surface temperature (SST) anomaly in the central equatorial Pacific (Wallace and Gutzler 1981). The PNA has been found to be a dominant mode of variation in the middle latitudes during the winter months. It has been shown to be strongly related to

TABLE 1. Canadian Reference Hydrometric Basin Network gauging stations used in the wavelet analysis. River drainage area and locations are included.

Region	Station	Latitude (°N)	Longitude (°W)	Drainage area (km^2)	Ecozone
			Eastern Canada		
1	02ZM006	47.6350	52.8372	3.63	Boreal Shield
1	02ZK001	47.2247	53.5683	285	Boreal Shield
1	02YR001	48.8078	54.2244	275	Boreal Shield
1	02ZH001	47.9469	54.2856	764	Boreal Shield
1	02YQ001	49.0153	54.8536	4400	Boreal Shield
1	02ZG001	47.2139	55.3292	205	Boreal Shield
1	02ZF001	47.7467	55.4417	1170	Boreal Shield
1	02YC001	50.6075	57.1511	624	Boreal Shield
1	02YL001	49.2406	57.3625	2110	Boreal Shield
1	02ZB001	47.6139	59.0092	205	Boreal Shield
1	02VC001	50.3078	63.6225	13 000	Boreal Shield
2	01FB001	46.3694	60.9767	368	Atlantic Maritime
2	01FB003	46.2233	61.1367	357	Atlantic Maritime
2	01EO001	45.1733	61.9817	1350	Atlantic Maritime
2	01DG003	44.8517	63.6650	96.9	Atlantic Maritime
2	01CA003	46.7442	64.1856	46.8	Atlantic Maritime
2	01EF001	44.4467	64.5917	1250	Atlantic Maritime
2	01BU002	45.9436	65.1703	391	Atlantic Maritime
2	01AP002	46.0719	65.3667	668	Atlantic Maritime
2	01EC001	43.8383	65.3700	495	Atlantic Maritime
2	01AP004	45.7019	65.6014	1100	Atlantic Maritime
2	01BO001	46.7361	65.8267	5050	Atlantic Maritime
2	01BQ001	47.0947	65.8372	948	Atlantic Maritime
2	01BP001	46.9358	65.9072	1340	Atlantic Maritime
2	01AQ001	45.1700	66.4667	239	Atlantic Maritime
2	01BE001	47.8317	66.8817	2270	Atlantic Maritime
2	01AK001	45.945	67.3222	234	Atlantic Maritime
2	01BC001	47.6667	67.4842	3160	Atlantic Maritime
2	01AD002	47.2569	68.5931	14 700	Atlantic Maritime
2	01AD003	47.2069	68.9569	1350	Atlantic Maritime
3	02PJ007	46.6592	71.2886	709	Mixed-wood plain
3	02OE027	45.4672	71.6553	642	Mixed-wood plain
3	02RD002	48.8994	72.2117	9320	Boreal Shield
3	02NF003	46.6858	73.9142	1390	Boreal Shield
3	02LB007	44.8422	75.5439	246	Mixed-wood plain
3	02KB001	45.8881	77.3083	4120	Boreal Shield
3	02HL004	44.5494	77.3292	712	Boreal Shield
3	02EC002	44.7128	79.2817	1520	Boreal Shield
3	02GA010	43.1906	80.4547	1030	Mixed-wood plain
3	02FB007	44.5225	80.9308	181	Mixed-wood plain
3	02FC001	44.4564	81.3267	3960	Mixed-wood plain
4	04NA001	48.6006	78.1094	3680	Boreal Shield
4	04LJ001	49.6167	83.2633	8940	Boreal Shield
4	04JC002	49.7789	84.5300	2410	Boreal Shield
4	02EA005	45.6694	79.3786	321	Boreal Shield
4	02AB008	48.3822	89.3078	187	Boreal Shield
4	02AA001	48.0122	89.6161	1550	Boreal Shield
			Central Canada		
5	05PB014	48.8500	92.7250	4870	Boreal Shield
5	06GD001	58.8917	96.2753	48 100	Taiga Shield
6	05LH005	51.8528	99.5472	55 000	Boreal Plain
			Western Canada		
7	08NF001	50.8861	116.0431	420	Montaine Cordillera
7	08NB005	51.4833	117.1792	9710	Montaine Cordillera
7	08NE087	49.4250	118.0417	80.5	Montaine Cordillera
7	08NE077	49.9075	118.1253	201	Montaine Cordillera
7	08LD001	50.9383	119.6544	3080	Montaine Cordillera
7	08LA001	51.6556	120.0653	10 200	Montaine Cordillera
7	08NL007	49.4597	120.5019	1850	Montaine Cordillera
7	08MH016	49.0839	121.4567	329	Pacific Maritime
7	08KH006	52.8436	122.2236	11 500	Montaine Cordillera
7	08MG005	50.3356	122.7994	2160	Pacific Maritime
7	08JE001	54.4181	124.2750	14 600	Montaine Cordillera

TABLE 1. *(Continued)*

Region	Station	Latitude (°N)	Longitude (°W)	Drainage area (km^2)	Ecozone
7	08JB002	54.0092	125.0050	3600	Montaine Cordillera
8	08MH006	49.2428	122.5783	37.3	Pacific Maritime
8	08GA010	49.3958	123.1444	172	Pacific Maritime
8	08HA003	48.7275	123.6697	209	Pacific Maritime
8	08HA001	48.8792	123.7019	355	Pacific Maritime
8	08HB008	49.2897	124.9103	347	Pacific Maritime
8	08HE006	50.0144	126.8425	181	Pacific Maritime
9	07FB001	55.7200	121.2078	12 100	Montaine Cordillera
9	10CD001	58.7883	122.6592	20 300	Taiga Plain, Boreal Cordillera
9	10CB001	57.2342	122.6942	2160	Taiga Plain, Boreal Cordillera
9	10BE004	58.8556	125.3806	2570	Boreal Cordillera
9	08CE001	57.9008	131.1544	29 300	Boreal Cordillera
9	08CG001	56.7389	131.6736	9350	Montaine Cordillera
9	09AE003	59.9306	131.7678	3320	Boreal Cordillera
9	09BA001	61.9944	132.3778	7250	Boreal Cordillera
9	09AA006	59.5992	133.8133	6810	Boreal Cordillera
9	09AC001	60.8522	135.7392	6990	Boreal Cordillera
9	09BC001	62.8297	136.5806	49 000	Boreal Cordillera

precipitation and temperature within the same season in the western United States (Redmond and Koch 1991). Strongly positive and negative PNA indices are associated with warm events (El Niño) and cold events (La Niña), respectively, and with North American precipitation and temperature anomalies (Yarnal and Diaz 1986). It has been found that the pressure anomalies associated with the different phases of the PNA alter the normal upper-atmospheric patterns, thus affecting temperature and precipitation patterns over various regions of North America (Shabbar et al. 1997a).

In addition to the NAO and PNA indices, indicators of the El Niño–Southern Oscillation (ENSO) are also selected for this study. The ENSO phenomenon is characterized as a spreading of warm water off the coast of South America from the equatorial central Pacific to eastern Pacific and is associated with climatic anomalies throughout the world. The ENSO index used in this study is the monthly mean equatorial Pacific SST time series over the Niño-3 region (5°N–5°S; 90°–150°W) (Rasmusson and Carpenter 1982). For notational simplicity, ENSO3 will be used herein to denote the SST series over that region. The influence of ENSO on streamflow is well documented (Redmond and Koch 1991; Kahya and Dracup 1993; Eltahir 1996) and subsequently the use of the ENSO–streamflow relationship for predictive purposes has been studied extensively in recent years (Moss et al. 1994; Piechota et al. 1998; Coulibaly et al. 2000; Gutiérrez and Dracup 2001).

It is noteworthy that some climatic indices are relatively interlinked over some time periods. A complex relationship has recently been shown between the NAO, ENSO, and PNA patterns (Huang et al. 1998). However, dynamical relationship between climatic patterns remains controversial and warrants further research (Diaz et al. 2001; Hurrell et al. 2003). Therefore, selected climatic patterns are used here as independent variables in order to assess the specific link between each climatic indictor and the Canadian seasonal streamflows.

3. Methods

The decomposition of time series into time–frequency space permits not only the identification of the dominant modes of variability, but also the determination of how these modes vary in time. This can be done by using either windowed Fourier transform or wavelet transform. However, a major shortcoming of standard Fourier transform is that it does not provide an accurate time–frequency localization of dynamical processes. A major advantage of using the wavelet transform over the Fourier transform is that wavelet analysis is scale independent (Kaiser 1994); hence there is no need for a predetermined scale (or response interval) that would limit the frequency range. Continuous wavelet transform is more appropriate for geophysical and hydrological time series because of the wide range of possible dominant frequencies. Moreover, it is also an efficient method for analyzing nonstationary signals (Daubechies 1990)—that property is particularly useful for analyzing complex time-varying patterns such as climatic indices and hydrological time series.

The wavelet analysis method described herein is limited to the needs of the present study. Emphasis is given to useful practical details for applying the method for hydrological time series analysis. For a more detailed description of wavelet analysis in geophysics and hydrology, readers are referred to other sources, such as Torrence and Compo (1998) and Labat et al. (2000b). The continuous wavelet transform W_n of a discrete sequence of observations x_n is defined as the convolution

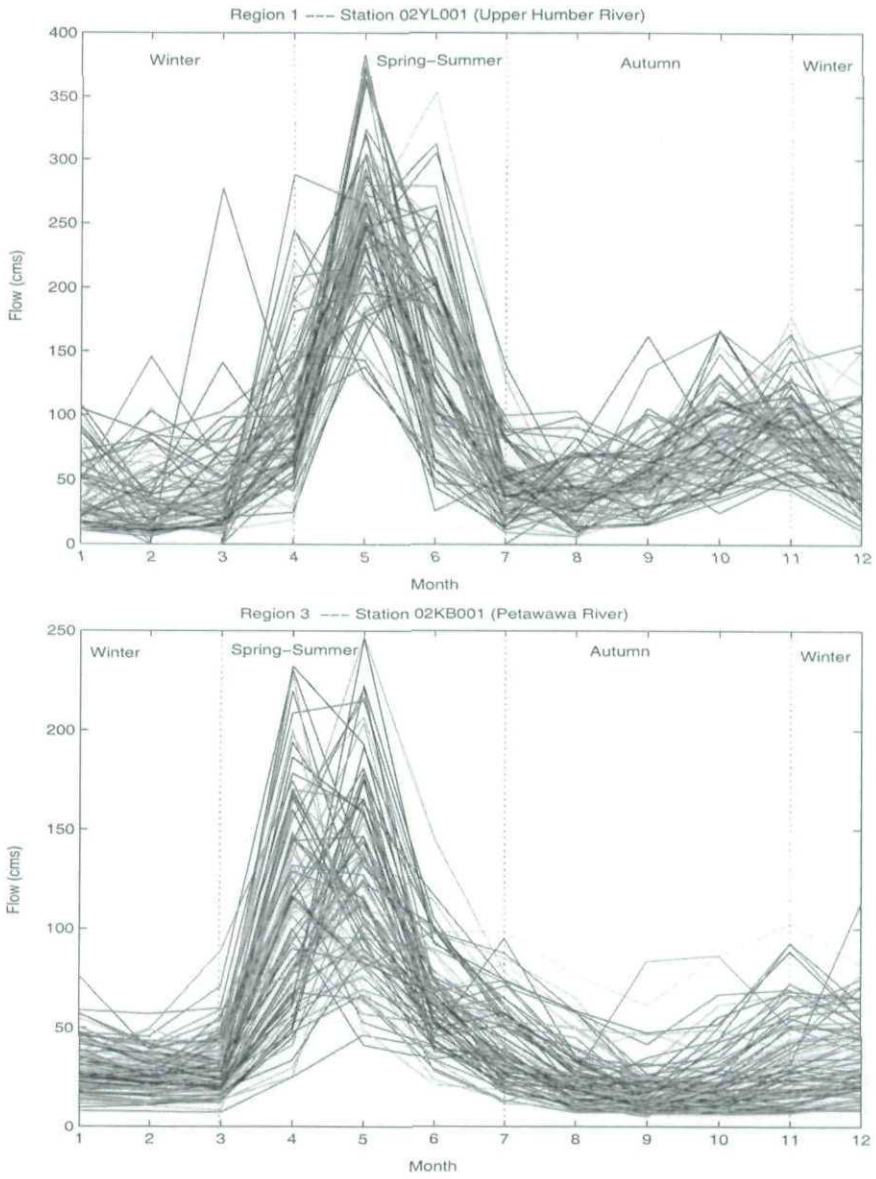

FIG. 2. Division of seasonal flows based on longer than 80-yr records.

of x_n with a scaled and translated wavelet $\psi(\eta)$ that depends on a nondimensional time parameter η,

$$W_n^X(s) = \sum_{n'=0}^{N-1} x_{n'} \psi^* \left[\frac{(n' - n)\delta t}{s} \right], \tag{1}$$

where n is the localized time index, s is the wavelet scale, δt is the sampling period, N is the number of points in the time series, and the asterik indicates the complex conjugate. Since complex wavelets lead to complex continuous wavelet transform, the wavelet power spectrum, defined as $|W_n(s)|^2$, is a convenient description of the fluctuation of the variance at different frequencies. Further, when normalized by σ^{-2} (where σ^2 is the variance), it gives a measure of the power relative to white noise since the expectation value for a white-noise process is σ^2 at all n and s. Figure 3b illustrates the normalized local wavelet power spectrum of a typical seasonal (autumn) streamflow time series (Fig. 3a) using the Morlet wavelet—a complex nonorthogonal wavelet consisting of a plane wave modulated by a Gaussian:

$$\psi_0(\eta) = \pi^{-0.25} e^{i\omega_0 \eta} e^{-0.5\eta^2}, \tag{2}$$

where ω_0 is the nondimensional frequency. The advantage of the Morlet wavelet over other candidates, such as the Mexican hat wavelet, resides in its good definition in the spectral space. For $\omega_0 = 6$ (used here), the Morlet wavelet scale is almost identical to the corre-

TABLE 2. Seasonal division of streamflow and climatic indices.

	Region	Winter	Spring–summer	Autumn
	1	Dec–Mar	Apr–July	Aug–Nov
East	2	Nov–Feb	Mar–July	Aug–Oct
	3	Dec–Feb	Mar–July	Aug–Nov
	4	Dec–Mar	Apr–July	Aug–Nov
Central	5	Dec–Apr	May–Aug	Sep–Nov
	6	Dec–Mar	Apr–Aug	Sep–Nov
	7	Dec–Apr	May–Aug	Sep–Nov
West	8	Nov–Mar	Apr–July	Aug–Oct
	9	Dec–Apr	May–Sep	Oct–Nov
			Indices*	
(ENSO3, NAO, PNA)		Dec–Mar	Apr–Jul	Aug–Nov

* Except for the Oct–Mar average ENSO3 indices, denoted ENSO3_OM (OM stands for Oct–Mar period).

sponding Fourier period of the complex exponential, and the terms *scale* and *period* may conveniently be used synonymously (Torrence and Compo 1998; Torrence and Webster 1999). Thus, the left axis in Fig. 3b is the equivalent Fourier period corresponding to the wavelet scale (henceforth called wavelet period), and the bottom axis is time (in years). The shaded contours are the normalized variance in excess of 1, 2, and 4. Features with variance larger than expected for a white-noise process reveal that the interannual variability is organized in preferential bands of wavelet periods. These bands, 2–3, 3–6, 6–12, and beyond 12 years, have been reported by other investigators in precipitation and streamflow time series (Rajagopalan and Lall 1998; Coulibaly et al. 2000; Anctil and Coulibaly 2004). This suggests the choice of the scale-averaged wavelet power to further examine fluctuations in power over specific ranges of wavelet periods (bands). Scale-averaged wavelet power is defined as the weighted sum of the wavelet power spectrum over scales s_1 to s_2:

$$\overline{W}_n^2 = \frac{\delta j \delta t}{C_\delta} \sum_{j=j_1}^{j_2} \frac{|W_n(s_j)|^2}{s_j}, \tag{3}$$

where δj is a factor that dictates the scale resolution (chosen as 0.1), and C_δ is a reconstruction factor specific to each wavelet form; $C_\delta = 0.776$ for the Morlet. This approach also allows increasing the degree of freedom of the power estimators. In Fig. 3, the dashed curve depicts the cone of influence of the wavelet analysis (Torrence and Compo 1998). Any peaks outside the cone of influence have presumably been reduced in magnitude due to the zero padding necessary to deal with finite-length observations. For example, it is possible that activity around a period of 16 yr in Fig. 3—see, for example Hu et al. (1998) for an exploration of such periods—carries on at both ends of the time series instead of diminishing as illustrated. However, for the span of the available streamflow data, it is not reasonable to consider wavelet periods much beyond 12

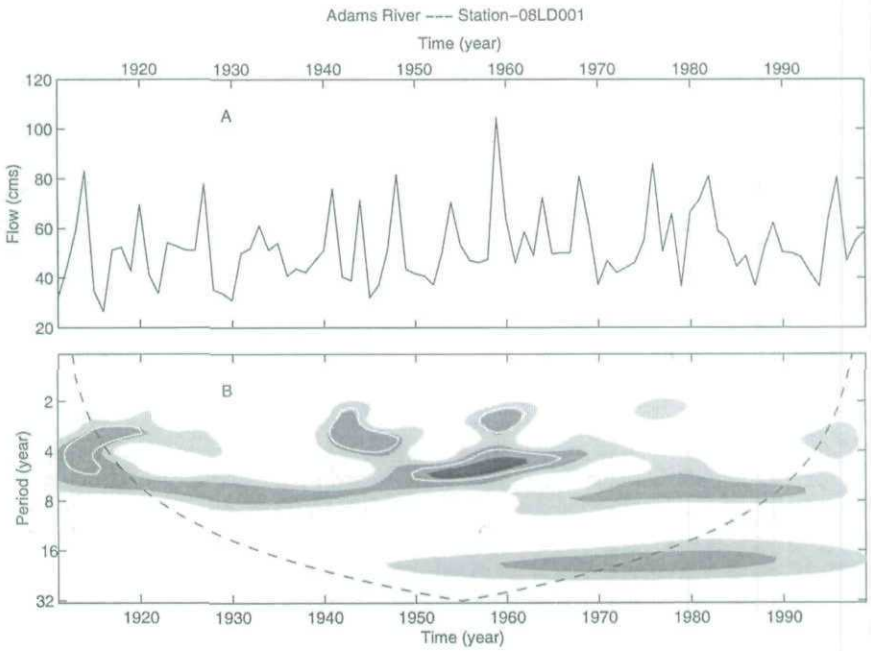

FIG. 3. Adams River (station 08LD001): (a) Time series of seasonal (autumn) streamflow. (b) Normalized local wavelet power spectrum of the autumn streamflow using the Morlet wavelet. The shaded contours are at normalized variance of 1, 2, and 4. Dashed curve depicts the cone of influence beyond which the edge effects become important. White contour lines enclose peaks of greater than 95% confidence for a red noise with a lag-1 coefficient α of 0.26.

yr. Three bands of wavelet periods are examined in greater detail: 2–3, 3–6, and 6–12. The power spectrum produced for a given time series is the product of the natural process involved and noise. The contour lines in Fig. 3 identify peaks of greater than 95% confidence for a red-noise process with a lag-1 coefficient α of 0.26 following the Monte Carlo analysis of Torrence and Compo (1998) based on the univariate lag-1 autoregressive process. It must not be presumed that regions of the power spectrum out of these 95% confidence level areas are the product of noise only. The natural process is also present in these regions, but influences the power spectrum to a lesser extent. The coefficient α is series specific and is estimated for each series.

Finally, cross-wavelet transforms are constructed to analyse the variability of the streamflow–climate relationship throughout Canada. The cross-wavelet power spectrum is defined as

$$|W_n^{XY}(s)| = |W_n^X(s)W_n^{Y*}(s)|, \quad (4)$$

where $W_n^{Y*}(s)$ is a the complex conjugate of $W_n^Y(s)$. It is normalized by $1/(\sigma_X\sigma_Y)$. The 95% confidence level follows the work of Torrence and Compo (1998). The Morlet wavelet cross-spectra permits one not only to depict the features common to both the climatic indices and the seasonal streamflows, but also to highlight temporal variations in their relationship.

4. Wavelet analysis results

a. *Power Hovmöller of Canadian seasonal streamflows*

The scale-average wavelet power represents the average variance ($\overline{\sigma^2}$) over a range of scales (or a certain band) and provides an efficient way to examine the fluctuations in power over a desired band. By averaging the wavelet power spectra at multiple locations, one can simultaneously assess the spatial and temporal variability of the streamflow data. Figure 4a shows a power Hovmöller (Torrence and Compo 1998), a time–longitude diagram of the normalized scale-averaged wavelet power for the streamflows in the 2–3-yr band at the longitude location of each hydrometric station. Shown in the figure are the results for the autumn, winter, and spring–summer seasons, as defined above. At each longitude, the wavelet power spectrum is computed using the Morlet wavelet, and the scale-averaged wavelet power over the 2–3-yr band is calculated. All scale-averaged wavelet power time series are then combined in a two-dimensional contour plot, with 95% confidence level computed using the lag-1 autocorrelation at each site. To allow the juxtaposition of streamflow from watersheds of different sizes, each scale-averaged series is normalized by σ^{-2} of the original series. The zonal average of the power Hovmöller (Fig. 4b) gives a measure of the average 2–3-yr variance of the streamflows and typically shows the temporal fluctuations of the streamflows over the entire area. For example, activities in the 2–3-yr band for autumn account for up to 50% of the average variance ($0.5\,\overline{\sigma^2}$) in the late 1920s, with moderate peaks ($0.40\,\overline{\sigma^2}$) around 1955 and 1978. In general, the autumn season streamflows demonstrate the most intense activity in the 2–3-yr band with moderate peaks in the 1950s and late 1970s, and a stronger peak in the 1920s. The winter season also demonstrates a strong peak in the 1920s and more moderate peaks in the 1930s and early 1980s. The spring–summer season corresponds to the least intense activity with only moderate peaks over several time periods.

Figure 5 presents similar results for the 3–6-yr band. Again, the autumn season exhibits the most intense activity with peaks in the 1920s, 1950s, and late 1970s. In comparison with the 2–3-yr band, the peaks are generally not as intense. The spring–summer period tends to exhibit more activity than the winter period for the 3–6-yr band in contrast to the results for the 2–3-yr band. Note also the very flat power spectrum for the winter season for the 3–6-yr band. Overall, the most striking feature, in the 2–3- and the 3–6-yr periods is a net distinction between the timing and intensity of the temporal variability in autumn, winter, and spring–summer streamflows—suggesting that these temporal structures are either driven by different climatic patterns or a phenomenon with significantly different seasonal intensity.

Figure 6 presents the results for the 6–12-yr band and reveals very little organized activity. This is likely at least in part an artifact of the limited length of data record available for analysis. As such, the 6–12-yr band will not be considered in the subsequent analyses.

b. *Seasonal streamflows and climatic patterns*

To determine coherent space–time variability in each of the three sectors (east, central, west—see Table 1) of the study area, principal component analysis is used. Figure 7 depicts the leading principal component for the stations from the east, central, and west portions of the study area. Results are shown for the autumn, winter, and spring–summer seasons. Noteworthy for all three seasons is the apparent change in behavior at around 1950. The indication of a change in response around 1950 will be explored further below. The somewhat flat response for the central region is again a manifestation of the limited number of long-term gauging stations available in the central region.

To visualize and examine the relationship between the seasonal streamflow and the selected climatic indices, Morlet wavelet cross-spectrum is calculated using the leading principal component of the seasonal flow and each of the selected climatic indices. Cross-wavelet spectrum permits highlighting of the streamflow–climate index covariance distribution across different time scales. Figures 8 to 11 present results for cross-wavelet analysis between climatic indices and seasonal streamflow. Results are presented for ENSO3,

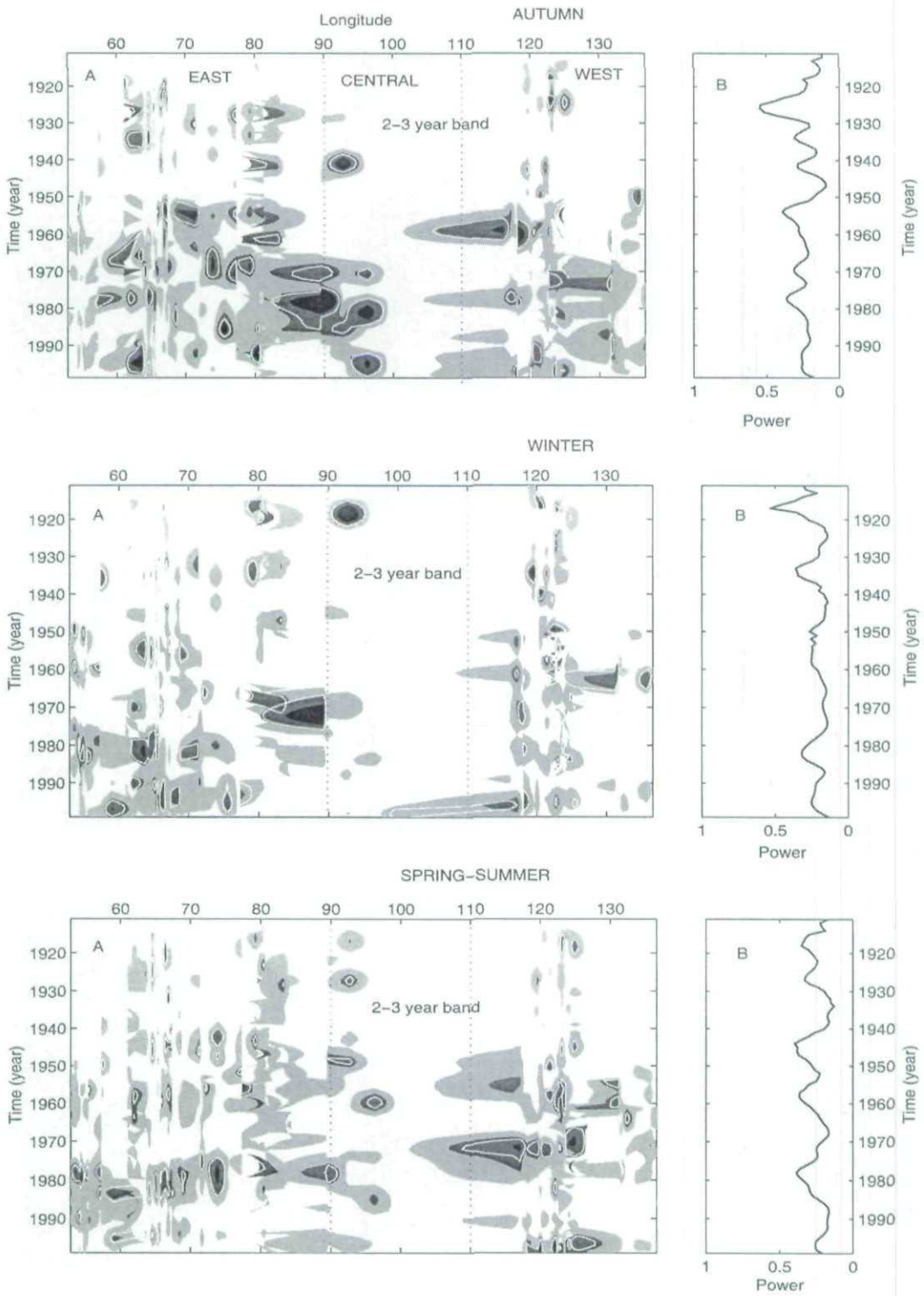

FIG. 4. Time–longitude diagrams of the seasonal flows in the 2–3-yr band. (a) Hovmöller plot of the normalized scale-averaged wavelet power. Shaded contours at normalized power of 0.2, 0.5, and 1. White contour lines enclose peaks of greater than 95% confidence computed using the lag-1 autocorrelation at each site. (b) Space averaged of the power Hovmöller.

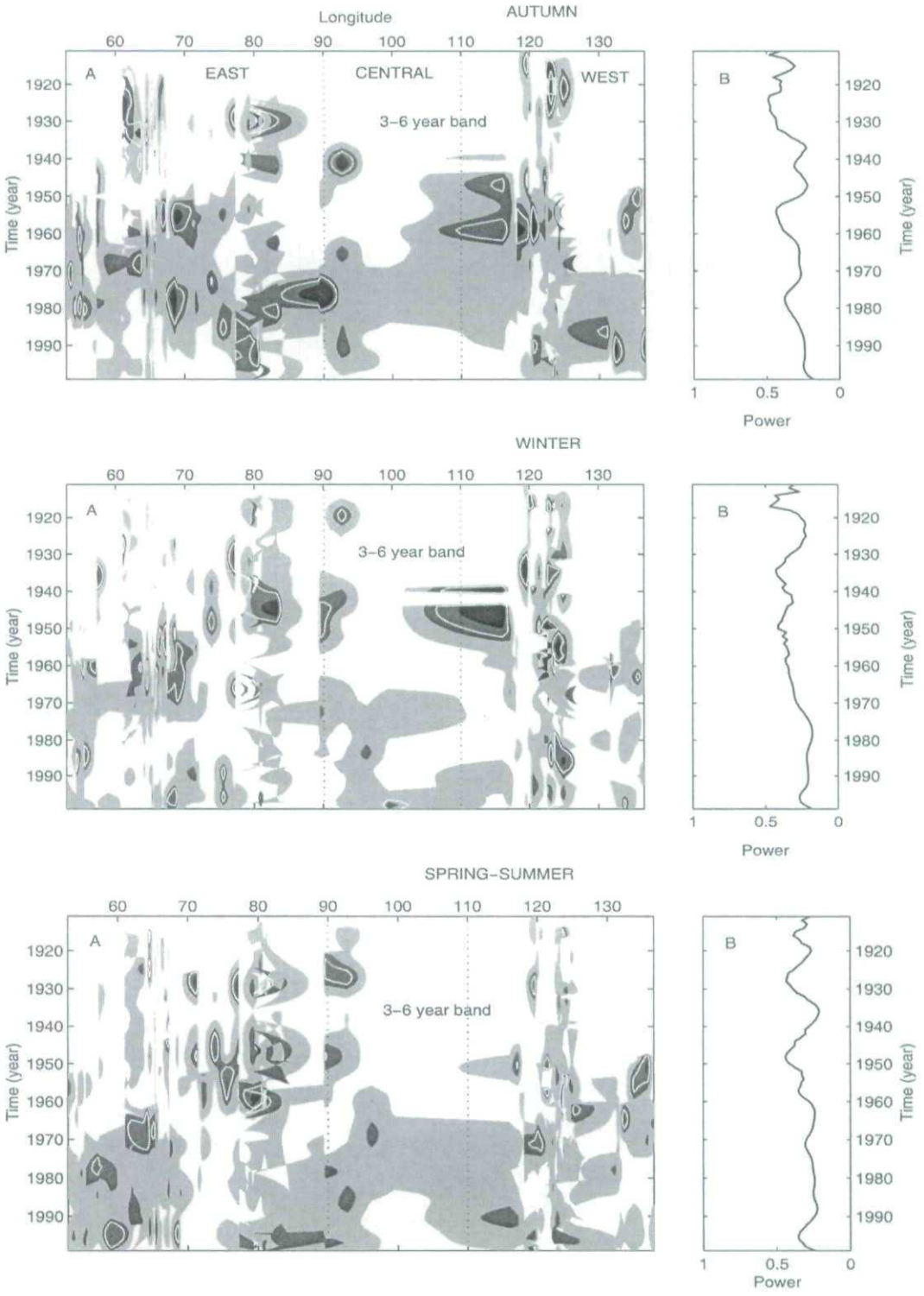

FIG. 5. Time–longitude diagrams of the seasonal flows in the 3–6-yr band. Features are identical to Fig. 4.

ENSO3_OM, NAO, and PNA. With the exception of the ENSO3_OM, each climatic index is presented for the same seasonal time period as the corresponding streamflow (see also the results in Table 2). The October to March average ENSO indices (namely ENSO3_OM) are commonly used as they cover the period when the ENSO signals are prominent. Note that the PNA series are available only from 1950, while the others are avail-

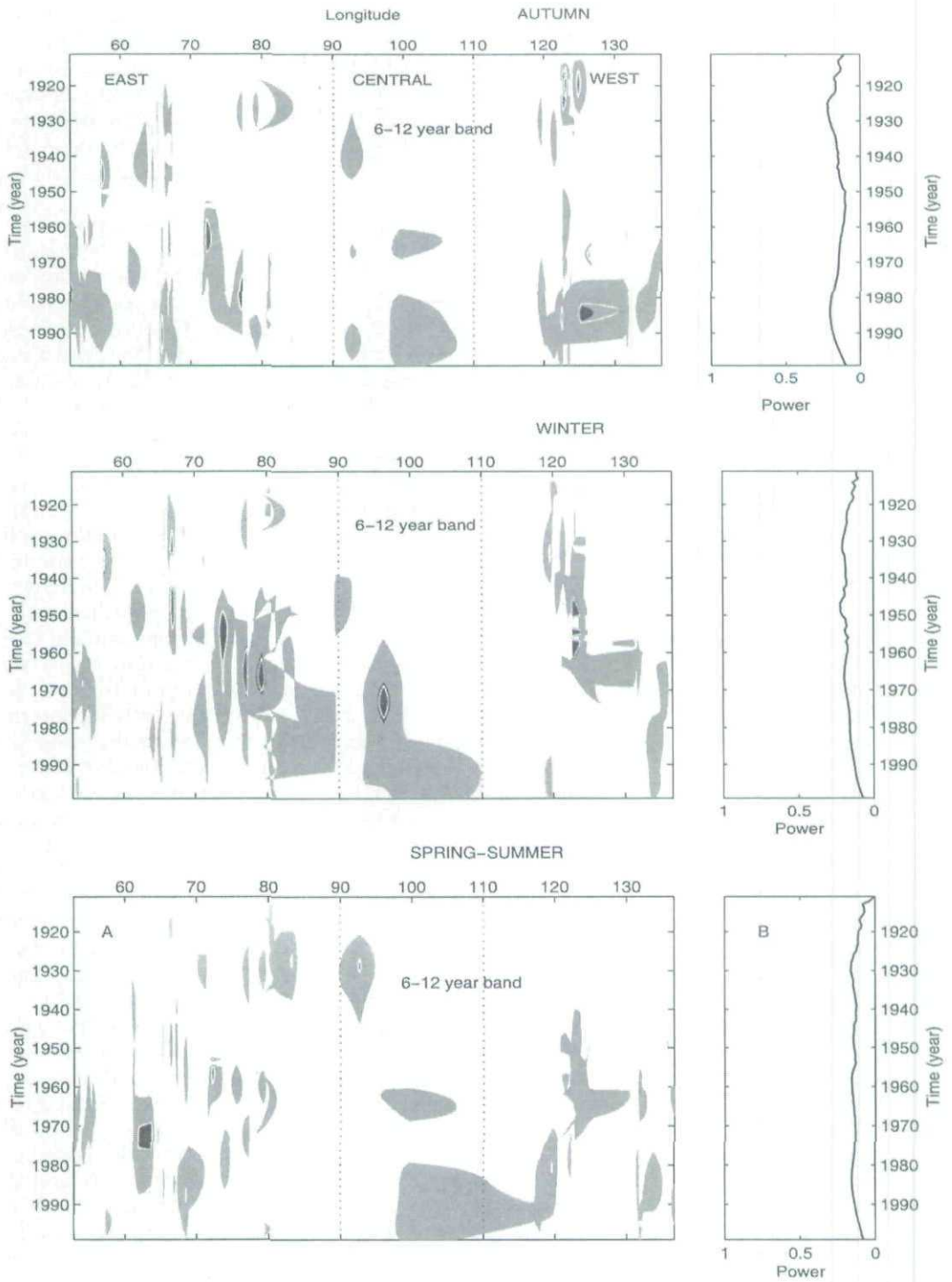

FIG. 6. Time–longitude diagrams of the seasonal flows in the 6–12-yr band. Features are identical to Fig. 4.

able for the entire study period (1911–99). Each of Figs. 8–11 shows the wavelet analysis for the climatic index in the top row with cross-wavelet analysis results for each sector (east, central, west) in the three following rows. The three columns present results for autumn, winter, and spring–summer, respectively. In each graph, the horizontal axis shows time (years) and the vertical axis shows the wavelet period (years).

The results for ENSO3 (Fig. 8) reveal the expected intense activity in the roughly 3–7-yr period that can be

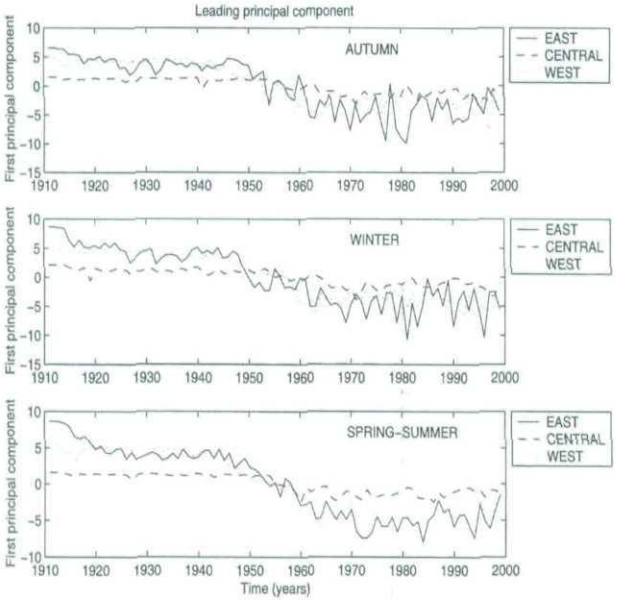

FIG. 7. Time series of the seasonal flow leading principal component: east, central, west.

anticipated for the ENSO phenomenon. Intense activity is noted in the 1980s and 1990s, the 1970s, and the 1940s. Stronger activity is noted for the autumn and winter seasons in comparison with the spring–summer season. The cross-wavelet analysis shows activity in the period from 1970 onwards with lesser activity noted for the spring–summer season. The activity in the cross-wavelet plots is concentrated in the roughly 2–7-yr period.

The results for ENSO3_OM (Fig. 9) are largely similar to those in Fig. 8 for ENSO3. The most noticeable difference with the ENSO3_OM analysis is the greater activity in the spring–summer season in comparison to the ENSO3 analysis. Correlations between ENSO3_OM and ENSO3 (spring–summer), ENSO3 (autumn), and ENSO3 (winter) are about 0.83, 0.68, and 0.95, respectively, for the 1910–99 period. In general, the wavelet cross-spectra (Figs. 8 and 9) do not show a particular advantage of using ENSO3_OM rather than the seasonal climatic indices.

Figure 10 presents the results for NAO. The top graphs show that the NAO results differ with the season in terms of the years with greater activity and the periods where the greatest activity is observed. Generally, the NAO is active in the 2–8-yr period but other periods also demonstrate intense activity (e.g., a longer period is observed for both the spring–summer and the autumn results). For the cross-wavelet analysis, the main activity is observed in the 2–6-yr period with stronger activity noted for the autumn and winter seasons in comparison to the spring–summer season.

The PNA results in Fig. 11 show areas of intense activity over a wider range of periods than was observed for the other climatic indices. In particular, there is a band of activity, especially noticeable in the spring–summer season, at a period of around 16 yr. The cross-wavelet analysis also exhibits intense activity over a wider range of periods with great variability in the results for different seasons and for different regions. This indicates that the PNA can be expected to have impacts on streamflow that will vary spatially and seasonally.

In general, the wavelet cross-spectra reveal stronger activity in the 2–6-yr period generally starting after 1950, particularly for the ENSO–streamflow and PNA–streamflow relationship. This can be associated with the well-documented shift in the atmospheric circulation around the mid-1970s over the Northern Hemisphere. However, a significant statistical relationship is observed between 1950 and 1970 in the ENSO–streamflow activity, particularly in autumn (Fig. 8). For the NAO–streamflow relationship, there is strong activity starting around the 1950s (Fig. 10), suggesting a possible role of the NAO in the 1950s shift in the streamflows. Only the PNA–streamflow activity appears stronger after 1970 except for the spring–summer season (Fig. 11). Prior to year 1950, there is only local and weaker 2–6-yr activity in central and western Canada essentially in winter and autumn (Figs. 8 and 9), but overall, there is no statistically significant streamflow–climate activity prior to 1950. The cross-wavelet analysis results consistently support the change point (around 1950) revealed by the principal component analysis and suggest that the shift in the seasonal Canadian streamflows around 1950s may more likely be related to the NAO index. Further discussion on the year 1950 change point is provided in section 5.

To further examine the dynamic relationship between the seasonal streamflow and the climatic indices, correlation analysis of the 2–6-yr power spectra are exploited. The correlation analysis also aims to assess possible time delay between seasonal indices and streamflows in the 2–6-yr band. Table 3 summarizes the results of correlation analysis between two climatic indices and the streamflow data. The results are presented for each of the three regions, for the three different seasons, and have also been summarized for the period before and after 1950 as well as for the entire period of record. Correlation values (Table 3) for the period after 1950 include not only the effects from the period after 1970, but also the effects of the period 1950–70. Therefore results in Table 3 should be interpreted along with Figs. 8–11, which highlight the temporal variation in the climate–streamflow relationship.

The east region demonstrates positive correlations with the ENSO in the spring–summer and winter seasons for the post-1950 period but much lower correlations for the period prior to 1950. In the period prior to 1950, the correlations tend to be negative with largest magnitudes noted for the autumn season. For the entire period of record, there is again a strong positive correlation with ENSO in winter and weaker, but still posi-

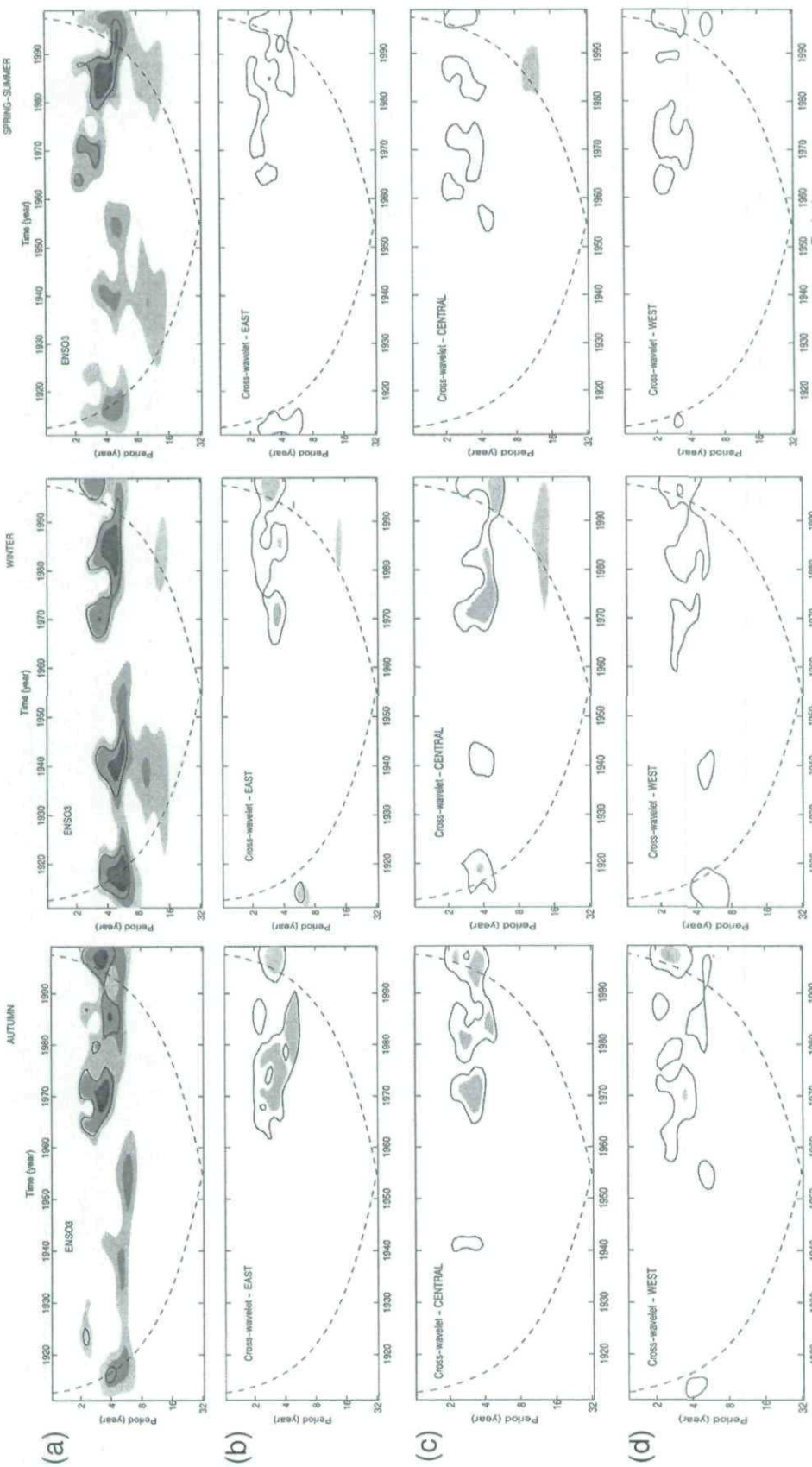

FIG. 8. (a) Normalized local wavelet spectrum of the seasonal ENSO3 index (autumn). Similar spectra are shown for the winter and spring–summer. The shaded contours are at normalized variance of 1, 2, and 4. The dashed curve depicts the cone of influence beyond which the edge effects become important. The contour lines enclose peaks of greater than 95% confidence. Normalized local cross-wavelet power spectra of the seasonal (autumn) flows and the seasonal (autumn) ENSO3 index for the (b) east, (c) central, and (d) west. Similar spectra are shown for the winter and the spring–summer.

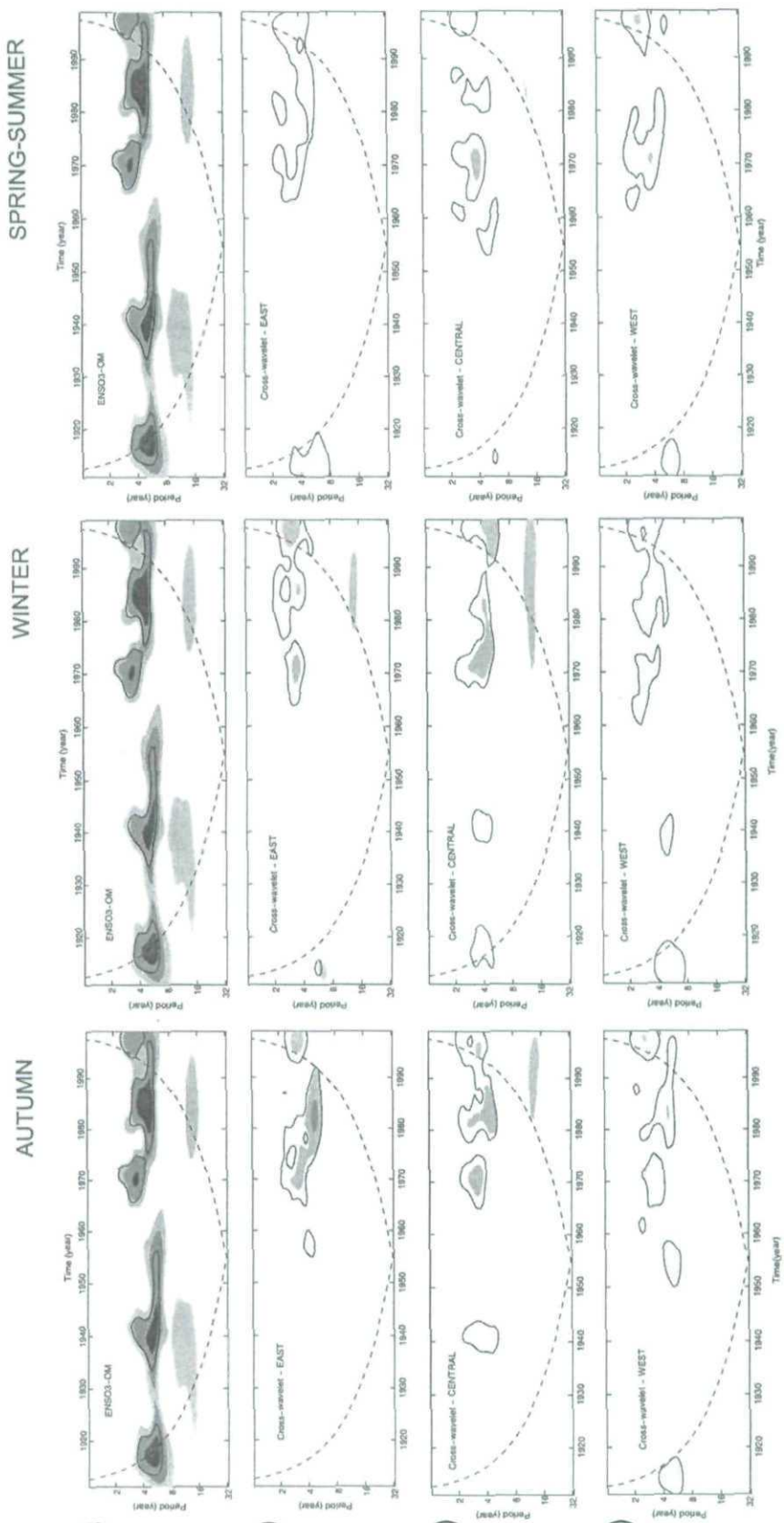

FIG. 9. Normalized local cross-wavelet power spectra of the seasonal flows and the Oct–Mar average ENSO3 indices. Features are identical to Fig. 8.

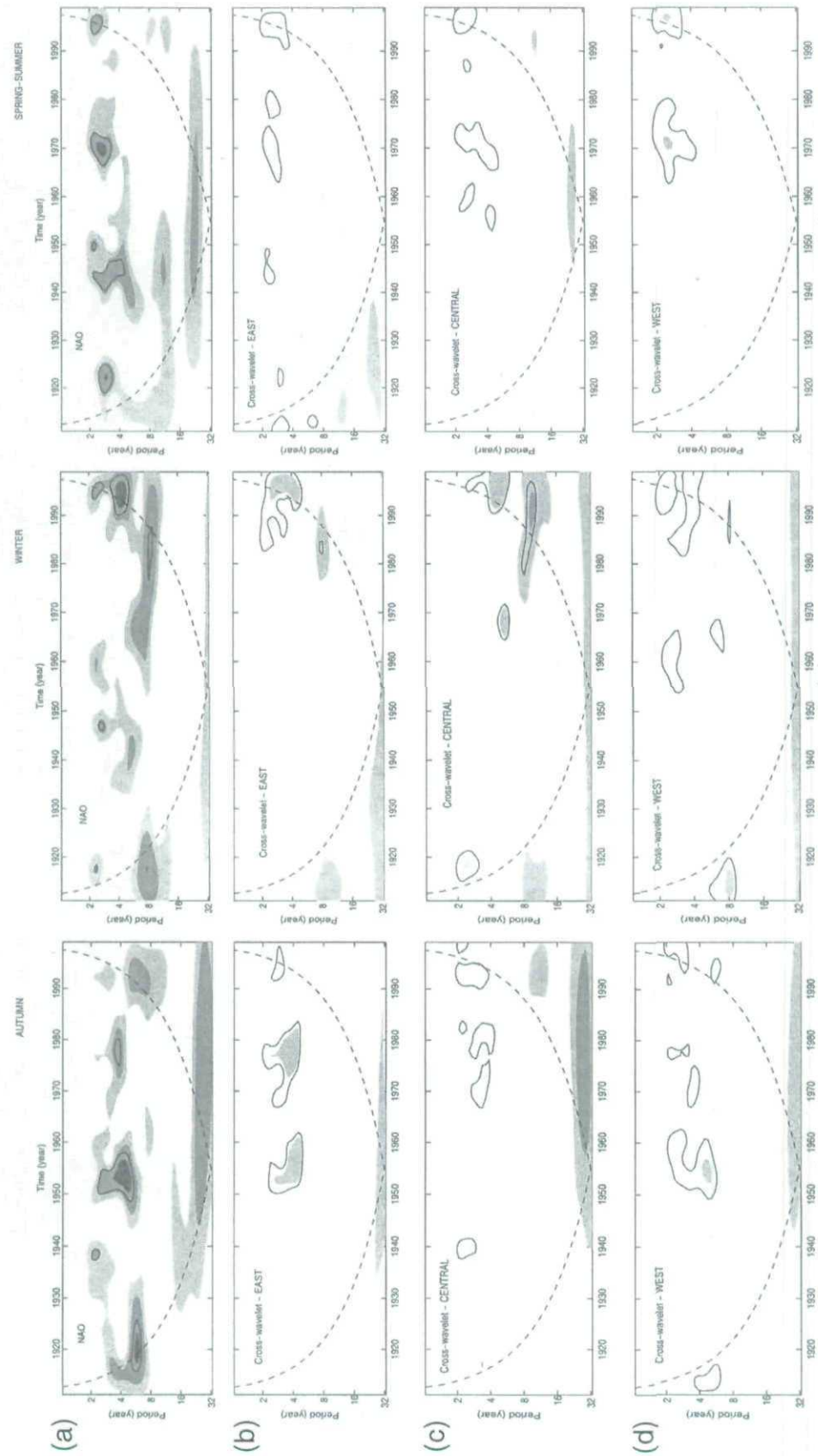

FIG. 10. Normalized local cross-wavelet power spectra of the seasonal flows and the seasonal NAO index. Features are identical to Fig. 8.

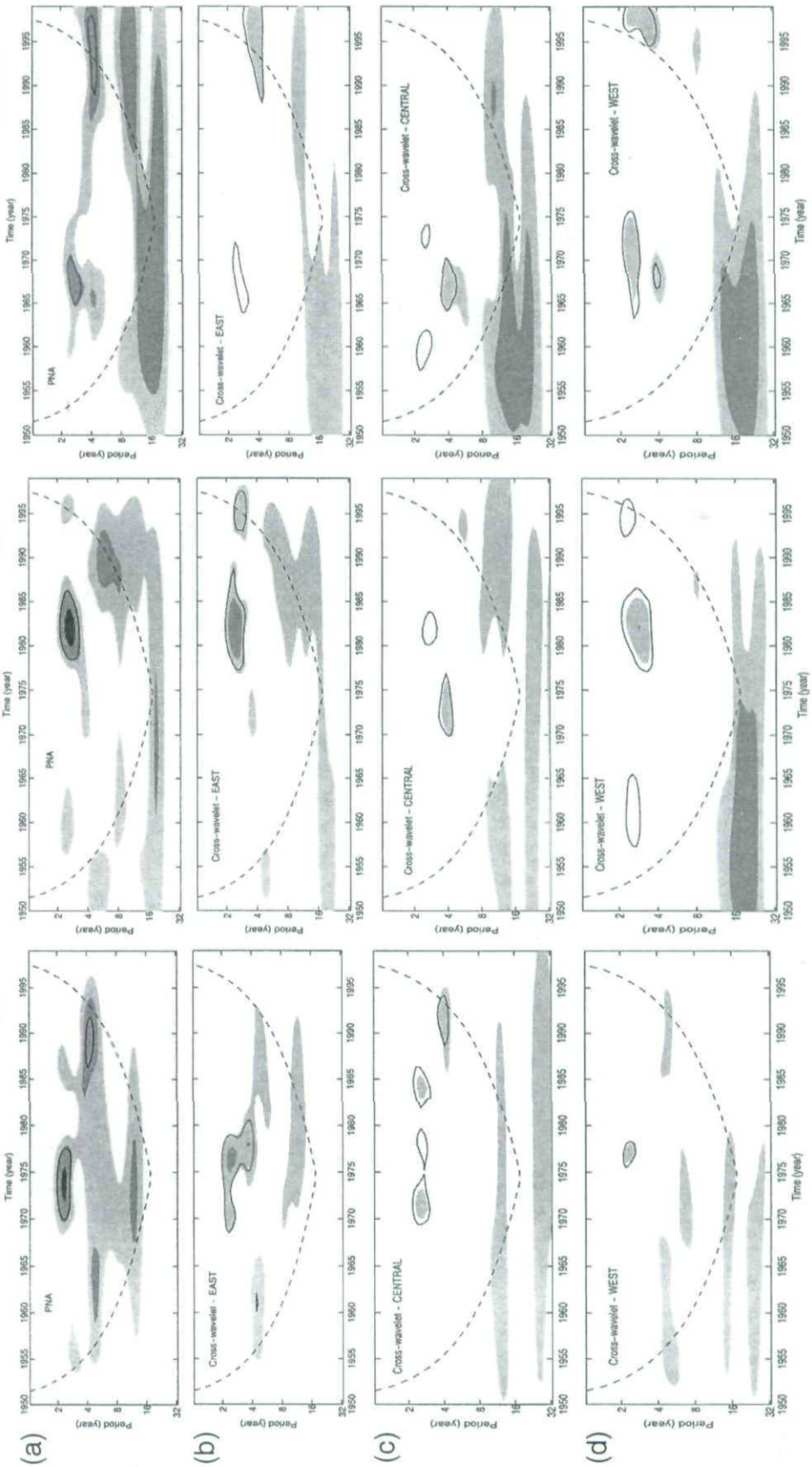

FIG. 11. Normalized local cross-wavelet power spectra of the seasonal flows and the seasonal PNA index. Features are identical to Fig. 8.

TABLE 3. Correlation analysis results for 2–6-yr band. Correlation values less than 0.30 are considered insignificant.

Indices	≤1950 flows			≥1950 flows			All (1911–99) flows		
	Spring–summer	Autumn	Winter	Spring–summer	Autumn	Winter	Spring–summer	Autumn	Winter
				East					
ENSO3_OM	−0.05	−0.42	−0.13	0.38	−0.10	0.48	0.18	0.04	0.35
ENSO3_win	−0.01	−0.39	−0.10	0.39	0.01	0.60	0.16	−0.01	0.33
ENSO3_spr–sum	0.09	−0.22	0.01	0.35	−0.14	0.54	0.31	0.19	0.58
ENSO3_aut	−0.08	−0.17	−0.12	0.39	−0.13	0.24	0.31	0.27	0.47
NAO_win	−0.03	−0.41	−0.06	0.75	−0.5	0.43	0.39	−0.15	0.40
NAO_spr–sum	−0.22	−0.57	−0.32	0.06	−0.07	−0.21	−0.15	−0.17	−0.24
NAO_aut	−0.18	0.02	−0.15	−0.38	−0.14	−0.39	−0.21	−0.03	−0.20
				Central					
ENSO3_OM	−0.15	0.58	0.55	−0.08	0.51	0.45	0.05	0.51	0.50
ENSO3_win	−0.13	0.48	0.68	−0.16	0.59	0.35	0.10	0.47	0.45
ENSO3_spr–sum	0.03	0.37	0.42	−0.15	0.42	0.02	0.17	0.52	0.20
ENSO3_aut	−0.04	0.14	0.67	0.19	0.29	0.78	0.44	0.46	0.72
NAO_win	0.01	−0.12	0.38	0.01	0.23	0.03	0.16	0.26	0.17
NAO_spr–sum	−0.30	0.33	0.08	0.04	0.01	0.72	−0.10	0.02	0.40
NAO_aut	−0.05	−0.39	0.22	−0.41	−0.39	−0.36	−0.23	−0.29	−0.18
				West					
ENSO3_OM	0.06	0.11	0.07	0.32	0.16	0.32	0.29	0.22	0.26
ENSO3_win	0.10	0.12	0.10	0.26	0.12	0.41	0.19	0.10	0.23
ENSO3_spr–sum	0.21	0.24	0.24	−0.04	−0.08	0.40	0.21	0.24	0.46
ENSO3_aut	0.04	−0.01	0.01	0.73	0.36	0.20	0.74	0.52	0.37
NAO_win	0.09	0.08	0.02	0.29	0.52	0.47	0.33	0.47	0.36
NAO_spr–sum	−0.23	−0.04	−0.27	0.49	0.08	−0.34	0.14	−0.04	−0.32
NAO_aut	−0.05	−0.17	−0.07	−0.37	−0.03	−0.52	−0.22	0.01	−0.23

tive, correlations with ENSO in spring–summer. A similar pattern emerges for the NAO in the east, although there is a positive correlation between the winter NAO and post-1950 and entire period streamflow and a negative correlation for the same time periods for the autumn NAO.

The central region demonstrates greater similarity in the results for the different time periods, as could be expected from the results in Fig. 7. Noteworthy is the strong, positive correlation for the autumn and winter seasons for the ENSO results. Strong, positive correlations are also observed for the spring–summer and winter seasons for the NAO results post-1950.

The west region demonstrates very little correlation in the period prior to 1950. In the post-1950 period, notable positive correlations include spring–summer and winter periods for ENSO and correlations for all seasons for the NAO. The entire period shows similar correlations to those for the post-1950 period, but with somewhat reduced magnitudes. A striking feature in the west is the significant change in correlations for both the ENSO3 and the NAO after 1950.

One of the most prominent features of the correlation analysis results is the consistently stronger and positive correlations for spring–summer and winter seasons for the ENSO3 results in western and eastern Canada since 1950—suggesting that the change (around 1950) observed in Fig. 7 and also suggested by Figs. 8 to 11—may also be related to the ENSO. A similar correlation pattern appears for NAO results in the west since 1950, while in the east negative correlations are observed for the autumn season prior to 1950. However, after 1950, strong NAO correlations emerge for all seasons in the east—suggesting a significant contribution of NAO in the seasonal streamflow variability in eastern and western Canada. Similar conclusions may not be drawn for central Canada owing to the limited number of stations, as discussed earlier.

5. Discussion

The main characteristic time scales (2–3- and 3–6-yr periods) of the seasonal streamflow revealed by the global wavelet spectra, along with the dominant patterns of the streamflow–climate variability identified by the cross-wavelet spectra, provide important information that is essential not only to any attempt to investigate the effects of climate change on Canadian streamflows, but also to improve seasonal streamflow prediction. Striking elements of the wavelet analysis results are the shift in the streamflows around 1950 (Figs. 7 and 4–6) and the absence of a significant statistical relationship between the streamflow and the climate indices prior to 1950. While the shift in Canadian annual streamflows around the 1970s has been well documented (Coulibaly and Burn 2004; Anctil and Coulibaly 2004; Perreault et al. 2000) and appears consistent with the shift in the atmospheric circulation

around 1970s in the Northern Hemisphere, the year 1950 change point revealed in the seasonal streamflows appears more likely related to NAO dynamics. The NAO–streamflow temporal relationship shown in Fig. 10 is consistent with the dynamics of the NAO during the last century (Hurrell et al. 2003): high values of the NAO in the early part (1900–30) of the century, low values during the period 1930–50 followed by a strong negative phase (1950–70—with extreme negative index around 1960s) and high positive values in the last 30 years (1970–2000—with highest values around 1990s). The strong streamflow/NAO activity around 1950 (Fig. 10) can be related to the shift of the NAO toward extremely negative phase, while the activity around year 1970 may be due to the second shift toward strongly positive NAO phase. The effect of the NAO on the streamflow appears particularly seasonal with a pronounced impact on autumn and spring–summer streamflows. This appears consistent with the dominant influence that the NAO exerts on temperature, precipitation, and storms of the Atlantic sector and surrounding continents (Marshall et al. 2001). Although the NAO is the dominant pattern of the atmospheric circulation variability over the North Atlantic, it explains only a fraction (about 31%) of the total variance—suggesting that other climatic patterns should be investigated in further analysis including the combination of climatic indices.

The second striking feature remains the absence of significant impact of climatic indices on the streamflows prior to 1950. A possible interpretation may include the effect of global warming. Global mean surface temperatures have risen between 0.3° and 0.6°C over the past century, including a warming of 0.2°–0.3°C since the 1950s when data are the most reliable (Houghton et al. 1995). Given that global mean temperatures are dominated by temperature variability over the northern continents (Terray and Cassou 2000), thus a significant part of the recent observed warming can be explained as a response to observed changes in atmospheric circulation—suggesting that the strong streamflow–climate activity after 1950 may be indirectly driven by the effect of global warming on low-frequency climate variability. Much more research is definitely needed to assert that assumption and to understand how the natural modes of low-frequency variability may be influenced by climate change. Further investigation should also include the temporal variability of the Canadian precipitation–climate relationship.

6. Conclusions

The continuous wavelet transform offers an effective tool for describing and quantifying the spatial and temporal variability of seasonal streamflows. Scale-averaged wavelet spectra permit the simultaneous assessment of the temporal and spatial variability in each of the three sets of 79 streamflow time series corresponding to winter, autumn, and spring–summer season. The span of the available streamflow records, 1911–99, allows the depiction of seasonal variance (or activity) for periods up to 12 years, thus three periods—namely 2–3, 3–6, and 6–12 yr bands—are investigated. It is shown that the Canadian seasonal streamflows are essentially dominated by the 2–3- and 3–6-yr activity with net differences between the timing and the intensity of the temporal variability in autumn, winter, and spring–summer. The 6–12-yr-band activity is dominated by white noise in all seasons. Cross-wavelet spectra revealed strong streamflow–climate activity in the 2–6-yr period starting after 1950 whatever the climatic index and the season. Prior to year 1950, only local and weaker 2–6-yr activity is revealed in central and western Canada essentially in winter and autumn. These results consistently support the change point (around 1950) revealed by the principal component analysis. It is found that the shift in the streamflow around 1950 is more likely related to the change in the NAO toward extremely negative phase.

Correlation analysis between streamflow activity and climatic pattern power in the 2–6-yr band revealed strong positive correlations with the ENSO and the NAO in the east region for spring–summer and winter seasons for the post-1950 period. In the period prior to 1950, the correlations tend to be negative with largest magnitudes noted for the autumn season. In the west region, there are no significant correlations prior to 1950. The major feature in the west is the strong correlation with both the ENSO and the NAO after 1950. The most prominent feature of the correlation analysis results is the consistently stronger and positive ENSO correlations in spring–summer and winter seasons in both western and eastern Canada since 1950—suggesting that the change point revealed around 1950 may also be related to the ENSO. The correlation analysis in the 2–6-yr band also suggests the presence of a change point around 1950 in the east and west seasonal streamflows. However, owing to the limited number of long-term stations available in the central region, similar conclusion cannot yet be drawn. Finally, a striking feature is the overall absence of significant statistical impact of the climatic indices on the seasonal streamflows prior to 1950. This may be related to the recent rise of the global mean temperatures; however, further investigation is needed to understand the relationship between low-frequency variability and climate change.

Acknowledgments. This work was made possible through grants from the Natural Sciences and Engineering Research Council of Canada to each author. The authors gratefully acknowledge the student contribution of Vanessa Arnold. The main wavelet analysis routines were provided by C. Torrence and G. P. Compo (available online at http://paos.colorado.edu/research/wavelets/). The NAO, PNA, and ENSO3 indices are available through the NOAA Climate Predic-

tion Center (URL http://www.cpc.ncep.noaa.gov/). The authors gratefully acknowledge the valuable comments of anonymous reviewers.

REFERENCES

Adamowski, K., and C. Bocci, 2001: Geostatistical regional trend detection in river flow data. *Hydrol. Processes,* **15,** 3331–3341.

Anctil, F., and P. Coulibaly, 2004: Wavelet analysis of the interannual variability in southern Quebec streamflow. *J. Climate,* **17,** 163–173.

Barnston, A. G., and R. E. Livezey, 1987: Classification, seasonality and persistence of low-frequency atmospheric circulation patterns. *Mon. Wea. Rev.,* **115,** 1083–1126.

Brown, R. D., and B. E. Goodison, 1996: Interannual variability in reconstructed Canadian snow cover, 1915–1992. *J. Climate,* **9,** 1299–1318.

Cayan, D. R., 1992: Latent and sensible heat flux anomalies over the northern oceans: The connection to monthly atmospheric circulation. *J. Climate,* **5,** 354–369.

Cook, E. R., R. D. D'Arrigo, and K. F. Briffa, 1998: A reconstruction of the North Atlantic Oscillation using tree-ring chronologies from North America and Europe. *The Holocene,* **8,** 1–9.

Coulibaly, P., and D. H. Burn, 2004: Wavelet analysis of variability in annual Canadian streamflows. *Water Resour. Res.,* **40,** 1–14.

——, F. Anctil, P. Rasmussen, and B. Bobée, 2000: A recurrent neural networks approach using indices of low-frequency climatic variability to forecast regional annual runoff. *Hydrol. Processes,* **14,** 2755–2777.

Daubechies, I., 1990: The wavelet transform time–frequency localization and signal analysis. *IEEE Trans. Inf. Theory,* **36,** 961–1004.

Diaz, H. F., M. P. Hoerling, and J. K. Eischeid, 2001: ENSO variability, teleconnections and climate change. *Int. J. Climatol.,* **21,** 1845–1862.

Eltahir, E. A. B., 1996: El Niño and the natural variability in the flow of the Nile River. *Water Resour. Res.,* **32,** 131–137.

Gutiérrez, F., and J. A. Dracup, 2001: An analysis of the feasibility of long-range streamflow forecasting for Colombia using El Niño–Southern Oscillation indicators. *J. Hydrol.,* **246,** 181–196.

Hameed, S., 1984: Fourier analysis of the Nile flood levels. *Geophys. Res. Lett.,* **11,** 843–845.

Harvey, K. D., P. J. Pilon, and T. R. Yuzyk, 1999: Canada's reference hydrometric basin network (RHBN). *Proc. CWRA 51st Annual Conf.,* Halifax, NS, Canada, Canadian Water Resources Association, CD-ROM.

Higuchi, K., J. Huang, and A. Shabbar, 1999: A wavelet characterization of the North Atlantic Oscillation variation and its relationship to the North Atlantic sea surface temperature. *Int. J. Climatol.,* **19,** 1119–1129.

Houghton, J. T., L. G. Meira Filho, J. Bruce, H. Lee, B. A. Callander, E. Haites, N. Harris, and K. Maskell, Eds., 1995: *Climate Change 1994: Radiative Forcing of Climate Change and an Evaluation of the IPCC IS92 Emission Scenarios.* Cambridge University Press, 339 pp.

Hu, Q., C. M. Woodruff, and S. E. Mudrick, 1998: Interdecadal variations of annual precipitation in the central United States. *Bull. Amer. Meteor. Soc.,* **79,** 221–229.

Huang, J., K. Higuchi, and A. Shabbar, 1998: The relationship between the North Atlantic Oscillation and the El Niño–Southern Oscillation. *Geophys. Res. Lett.,* **25,** 2707–2710.

Hurrell, J. W., 1995: Decadal trends in the North Atlantic Oscillation: Regional temperature and precipitation. *Science,* **269,** 676–679.

——, Y. Kushnir, G. Ottersen, and M. Visbeck, Eds., 2003: *The North Atlantic Oscillation: Climate Significance and Environmental Impact, Geophys. Monogr.,* No. 134, Amer. Geophys. Union, 279 pp.

Kahya, E., and J. A. Dracup, 1993: U.S. streamflow patterns in relation to the El-Niño/Southern Oscillation. *Water Resour. Res.,* **29,** 2491–2503.

Kaiser, G., 1994: *A Friendly Guide to Wavelets.* Birkhäuser, 300 pp.

Kumar, P., 1996: Role of coherent structure in the stochastic dynamic variability of precipitation. *J. Geophys. Res.,* **101,** 393–404.

——, and E. Foufoula-Georgiou, 1993: A multicomponent decomposition of spatial rainfall fields. Part 1: Segregation of large and small scale features using wavelet transforms. *Water Resour. Res.,* **29,** 2515–2532.

Kunhel, I., T. A. McMahon, B. L. Finlayson, A. Haines, P. H. Whetton, and T. T. Gibson, 1990: Climatic influences on streamflow variability: A comparison between southeastern Australia and southeastern United States of America. *Water Resour. Res.,* **26,** 2483–2496.

Labat, D., R. Ababou, and A. Mangin, 2000a: Rainfall–runoff relations for karstic springs. Part I: Convolution and spectral analyses. *J. Hydrol.,* **238,** 123–148.

——, ——, and ——, 2000b: Rainfall–runoff relations for karstic springs. Part II: Continuous wavelet and discrete orthogonal multiresolution analyses. *J. Hydrol.,* **238,** 149–178.

Larocque, M., A. Mangin, M. Razack, and O. Banton, 1998: Contribution of correlation and spectral analysis to the regional study of the large karst aquifer (Charente, France). *J. Hydrol.,* **205,** 217–231.

Lucero, O. A., and N. C. Rodriguez, 1999: Relationship between interdecadal fluctuations in annual rainfall amount and annual rainfall trend in a southern mid-latitudes region of Argentina. *Atmos. Res.,* **52,** 177–193.

Marshall, J., and Coauthors, 2001: North Atlantic climate variability: Phenomena, impacts and mechanisms. *Int. J. Climatol.,* **21,** 1863–1898.

Moss, M. E., C. P. Pearson, and A. I. McKerchar, 1994: The Southern Oscillation index as a predictor of the probability of low streamflows in New Zealand. *Water Resour. Res.,* **30,** 2717–2724.

National Research Council, 1998: *Decade-to-Century-Scale Climate Variability and Change: A Science Strategy.* National Academy Press, 142 pp.

Perreault, L., J. Bernier, B. Bobee, and E. Parent, 2000: Bayesian change point analysis in hydrometeorological time series: Part 1. The normal model revised. *J. Hydrol.,* **235,** 221–241.

Piechota, T. C., F. H. S. Chiew, and J. A. Dracup, 1998: Seasonal streamflow forecasting in eastern Australia and the El-Niño-Southern Oscillation. *Water Resour. Res.,* **34,** 3035–3044.

Rajagopalan, B., and U. Lall, 1998: Interannual variability in western US precipitation. *J. Hydrol.,* **210,** 51–67.

Rasmusson, E. M., and T. H. Carpenter, 1982: Variations in tropical sea surface temperature and surface wind fields associated with the Southern Oscillation/El Niño. *Mon. Wea. Rev.,* **110,** 354–384.

Redmond, K. T., and R. W. Koch, 1991: Surface climate and streamflow variability in the western United States and their relationships to large-scale circulation indices. *Water Resour. Res.,* **27,** 2381–2399.

Shabbar, A., B. Bonsal, and M. Khandekar, 1997a: Canadian precipitation patterns associated with the Southern Oscillation. *J. Climate,* **10,** 3016–3027.

——, K. Higuchi, W. Skinner, and J. L. Knox, 1997b: The association between the BWA index and winter surface temperature variability over eastern Canada and west Greenland. *Int. J. Climatol.,* **17,** 1195–1210.

Smith, L. C., D. Turcotte, and B. L. Isacks, 1998: Stream flow characterization and feature detection using a discrete wavelet transform. *Hydrol. Processes,* **12,** 233–249.

Szilagyi, J., M. B. Parlange, G. G. Katul, and J. D. Albertson,

1999: An objective method for determining principal time scales of coherent eddy structures using orthogonal wavelets. *Adv. Water Resour.*, **22,** 561–566.

Takeuchi, N., K. Narita, and Y. Goto, 1994: Wavelet analysis of meteorological variables under thunderclouds over the Japan sea. *J. Geophys. Res.*, **99** (D5), 10 751–10 757.

Terray, L., and C. Cassou, 2000: Modes of low-frequency climate variability and their relationships with land precipitation and surface temperature: Application to the Northern Hemisphere winter climate. *Stochastic Environ. Res. Risk Assess.*, **14,** 339–368.

Torrence, C., and G. P. Compo, 1998: A practical guide to wavelet analysis. *Bull. Amer. Meteor. Soc.*, **79,** 61–78.

——, and P. J. Webster, 1999: Interdecadal changes in the ENSO–monsoon system. *J. Climate,* **12,** 2679–2690.

Wallace, J. M., and D. S. Gutzler, 1981: Teleconnections in the geopotential height field during the Northern Hemisphere winter. *Mon. Wea. Rev.*, **109,** 784–812.

Yarnal, B., and H. F. Diaz, 1986: Relationships between the extremes of the Southern Oscillations and the winter climate of the Anglo–American Pacific coast. *Int. J. Climatol.*, **6,** 197–219.